Article

Cell Reports

Mesenchymal Transition of High-Grade Breast Carcinomas Depends on Extracellular Matrix Control of Myeloid Suppressor Cell Activity

Graphical Abstract

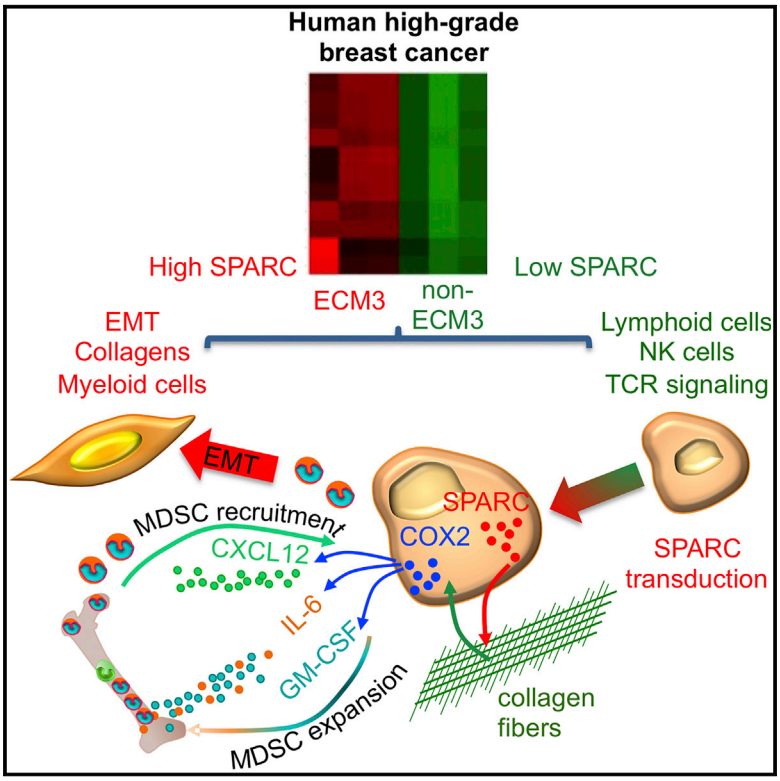

Highlights

- In breast cancer, the extracellular matrix can impact the immune microenvironment
- Suppressive activity of myeloid cells is required for EMT of breast cancer cells
- Interrupting ECM-MDSCs crosstalk can revert EMT and restore chemosensitivity

Authors

Sabina Sangaletti, Claudio Tripodo, Alessandra Santangelo, ..., Elda Tagliabue, Claudia Chiodoni, Mario P. Colombo

Correspondence

sabina.sangaletti@istitutotumori.mi.it (S.S.), mariopaolo.colombo@istitutotumori.mi.it (M.P.C.)

In Brief

Sangaletti et al. show that in high-grade breast cancer, the mesenchymal transition depends on extracellular matrix (ECM)-mediated control of myeloid-derived suppressor cell (MDSC) activity. Interrupting this ECM-MDSC crosstalk with aminobisphosphonates can revert the EMT to restore chemosensitivity.

Accession Numbers

GSE59590

Sangaletti et al., 2016, Cell Reports *17*, 233–248
September 27, 2016
http://dx.doi.org/10.1016/j.celrep.2016.08.075

Cell Reports
Article

Mesenchymal Transition of High-Grade Breast Carcinomas Depends on Extracellular Matrix Control of Myeloid Suppressor Cell Activity

Sabina Sangaletti,[1,4,*] Claudio Tripodo,[2] Alessandra Santangelo,[1] Nadia Castioni,[1] Paola Portararo,[1] Alessandro Gulino,[2] Laura Botti,[1] Mariella Parenza,[1] Barbara Cappetti,[1] Rosaria Orlandi,[3] Elda Tagliabue,[3] Claudia Chiodoni,[1] and Mario P. Colombo[1,*]

[1]Molecular Immunology Unit, Department of Experimental Oncology and Molecular Medicine, Fondazione IRCCS Istituto Nazionale Tumori, 20133 Milan, Italy

[2]Tumor Immunology Unit, Human Pathology Section, Department of Health Science, Palermo University School of Medicine, 90129 Palermo, Italy

[3]Molecular Targets Unit, Department of Experimental Oncology and Molecular Medicine, Fondazione IRCCS Istituto Nazionale dei Tumori, 20133 Milan, Italy

[4]Lead Contact

*Correspondence: sabina.sangaletti@istitutotumori.mi.it (S.S.), mariopaolo.colombo@istitutotumori.mi.it (M.P.C.)

http://dx.doi.org/10.1016/j.celrep.2016.08.075

SUMMARY

The extracellular matrix (ECM) contributes to the biological and clinical heterogeneity of breast cancer, and different prognostic groups can be identified according to specific ECM signatures. In high-grade, but not low-grade, tumors, an ECM signature characterized by high SPARC expression (ECM3) identifies tumors with increased epithelial-to-mesenchymal transition (EMT), reduced treatment response, and poor prognosis. To better understand how this ECM3 signature is contributing to tumorigenesis, we expressed SPARC in isogenic cell lines and found that SPARC overexpression in tumor cells reduces their growth rate and induces EMT. SPARC expression also results in the formation of a highly immunosuppressive microenvironment, composed by infiltrating T regulatory cells, mast cells, and myeloid-derived suppressor cells (MDSCs). The ability of SPARC to induce EMT depended on the localization and suppressive function of myeloid cells, and inhibition of the suppressive function MDSCs by administration of aminobisphosphonates could revert EMT, rendering SPARC-overexpressing tumor cells sensitive to Doxil. We conclude that that SPARC is regulating the interplay between MDSCs and the ECM to drive the induction of EMT in tumor cells.

INTRODUCTION

As part of the tumor stroma, immune cells participate in neoplastic transformation and co-evolve with malignancies through a bi-directional crosstalk. The understanding of the mechanisms that govern this crosstalk could contribute to the identification of an approach to interrupt this interplay (Hanahan and Coussens, 2012). Non-cellular components of the microenvironment such as the extracellular matrix (ECM) also contribute to many aspects of tumor progression. For example, increased collagen deposition and augmented ECM stiffness can impact integrin signaling and promote tumor cell survival and proliferation (Lu et al., 2012).

The regulatory role of the ECM can extend to the immune cell compartment and abnormal ECM composition or organization may impact immune cell infiltration, differentiation, and function (Lv et al., 2013). Indeed, non-structural matricellular proteins, and in particular secreted protein acidic and rich in cysteine (SPARC), have emerged as master regulators of stromal remodeling (Brekken and Sage, 2001). M2-macrophages are often recruited into the tumor microenvironment, where they can help sustain tumor growth and promote metastasis, for example. In SPARC-deficient mice, decreased collagen deposition results in increased recruitment of infiltrating inflammatory (M1) macrophages, suggesting that modifications of the ECM may simultaneously influence the number and function of immune cells (Sangaletti et al., 2003).

In addition to macrophages, altered ECM composition can impact other myeloid populations such as neutrophils. Importantly, their homeostasis is affected by SPARC-mediated regulation of ECM assembly at both central and peripheral sites, as both the myelopoietic potential of bone marrow (BM) and the granulocytic infiltration of peripheral tissues are influenced by stromal SPARC expression (Sangaletti et al., 2014b; Tripodo et al., 2012).

During tumorigenesis, myeloid-derived suppressor cells (MDSCs) can be licensed from the BM (Bronte et al., 2016). MDSCs have been shown to promote tumor invasiveness by supporting epithelial-to-mesenchymal transition (EMT) (Toh et al., 2011). This evidence suggests that the EMT is determined not only by tumor cell-intrinsic events but also by the quality of immune cells populating the tumor stroma.

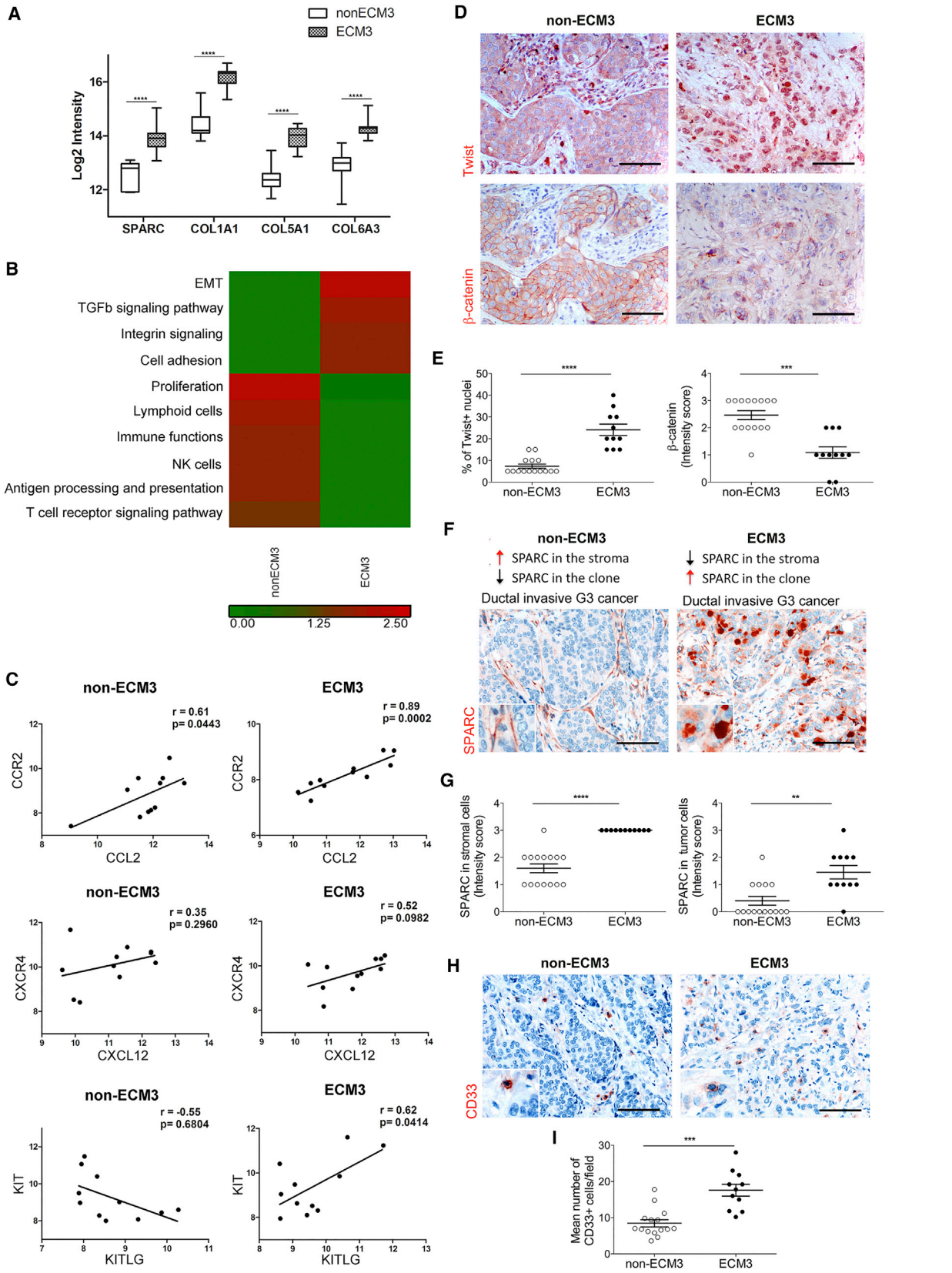

(legend on next page)

Depending on their EMT status, mammary tumors display different ECM composition. Indeed, breast cancer prognostic groups can be identified according to differences in enrichment of ECM genes, leading to the identification of four specific ECM signatures (ECM0–ECM3) (Bergamaschi et al., 2008). Among these signatures, ECM3, which is characterized by high *Sparc* expression, is found in ~35% of breast carcinomas and is associated with high-grade tumors with increased EMT features and poor response to therapy (Triulzi et al., 2013). This suggests that the interaction between the tumor and the ECM may influence tumor progression. However, the mechanisms responsible for the association between ECM composition and tumor grade remain largely unknown. In this study, we investigate the concomitant activity of the ECM gene *Sparc* in regulating the quality of the tumor-associated ECM and directing the infiltrating immune cells to determine the cancer phenotype and behavior.

RESULTS

ECM and EMT Cancer Characteristics Correlate with Myeloid Cell Infiltration and Localization

To determine whether the ECM profile correlates with tumor differentiation and grading, EMT characteristics, and immune response, we performed unsupervised clustering on ECM-related genes to classify ECM3 and non-ECM3 tumors according to Triulzi and colleagues (Triulzi et al., 2013) using whole frozen tissues from 97 consecutive primary breast tumors (Huang et al., 2015). This classification, together with histological grading, subdivided the 97 cases cohort into 11 high-grade ECM3, 37 high-grade non-ECM3, 20 low-grade ECM3, and 24 low-grade non-ECM3 tumors. Five cases were excluded due to unclear ECM classification or the absence of data on tumor grade. Considering the capacity of the ECM3 signature to interrelate with the tumor grade, which is prognostic in high-grade tumors, but not low-grade tumors (Triulzi et al., 2013), we focused our analysis on ECM3 and non-ECM3 high-grade tumors. Gene expression profile (GEP) analysis showed that high-grade ECM3 tumors were characterized by a significant increase in the expression of SPARC and 13 collagen genes, including COL1A1, COL5A1, and COL6A3 (Bergamaschi et al., 2008) (Figure 1A; $p < 0.0001$). Focusing on the ECM3 high-grade fraction, we observed enrichment of genes belonging to the EMT, transforming growth factor β, integrin signaling, and cell adhesion pathways (Figure 1B). In contrast, high-grade non-ECM3 tumors were characterized by overexpression of proliferation genes. Moreover, high-grade ECM3 and non-ECM3 tumors also differed in the expression of genes related to immune functions, with ECM3 tumors being deficient in natural killer (NK), T, and B cell-related genes, which were enriched in their non-ECM3 counterparts (Figure 1B; Table S1). Myeloid-related genes were expressed at comparable levels in high-grade ECM3 and non-ECM3 tumors, with high expression of myeloid-related genes such as CD33, KIT, KITLG, TNF, CCL5, IL6, IL8, IL10, CCL2, CXCL12, CCR2, and CXCL4 (Figure S1A). However, the analysis of ligand/receptor pairs that identify pathways by function (Murdoch et al., 2008) showed that the CCL2/CCR2, CXCR4/CXCL12, and KITLG/KIT pairs were significantly correlated with ECM3 tumors (Figure 1C).

In support of the results of gene set enrichment analysis (GSEA), immunohistochemical analysis performed on all 11 available ECM3 high-grade cases and 15 out of 37 non-ECM3 high-grade cases showed predominant EMT characteristics in the high-grade ECM3 tumors, with Twist mainly localizing in the nucleus and β-catenin being reduced or confined to the cytoplasm rather than localized at the cellular membrane (Figures 1D, 1E, and S1B; Table S2). High-grade ECM3 and non-ECM3 tumors can be further classified on the basis of SPARC immunolocalization in both stroma and neoplastic cells or mostly in the stroma cell component, respectively (Figures 1F, 1G, and S1B; Table S2). Moreover, SPARC expression in neoplastic cells was associated with the enrichment of infiltrating $CD33^+$ myeloid cells in direct contact with cancer cells (Figures 1H, 1I, and S1B; Table S2). In contrast, the cases in which SPARC was confined to the stroma were characterized by a paucity of $CD33^+$ myeloid

Figure 1. The ECM Characteristics Determine the Interaction between Tumor and Myeloid Cells and the Enrichment of EMT Features

(A) Expression of SPARC and collagen 1A1, 5A1, and 6A3 mRNAs (representative of the 13 collagen genes of the ECM3 signature; Triulzi et al., 2013) in high-grade ECM3 and non-ECM3 breast cancer samples from the Huang dataset (Huang et al., 2015). The expression levels of SPARC and collagen genes are significantly higher in ECM3 tumors than in non-ECM3 tumors (Mann-Whitney *U* test, $p < 0.0001$). Box and whisker plots: the bottom and the top of the box represent the first and third quartiles, and the band inside the box is the median. The ends of the whiskers represent the minimum and maximum of all data.

(B) Functional profile of high-grade breast carcinomas according to ECM characteristics through gene set enrichment analysis (GSEA). The heatmap shows the normalized enrichment scores (NES) of significantly enriched gene sets (nominal p value < 0.05, FDR *q*-value < 0.20) in grade III non-ECM3 and grade III ECM3 breast cancer samples from the Huang dataset (Huang et al., 2015).

(C) Pearson correlation analysis of gene expression levels of distinctive ligand/receptor pairs in MDSCs in non-ECM3 (left) and ECM3 (right) breast cancer samples.

(D) IHC analysis of Twist and β-catenin in ECM3 and non-ECM3 tumors indicates enrichment of EMT characteristics in high-grade ECM3 tumors, where Twist is mainly localized in the nucleus and β-catenin is mainly expressed in the cytoplasm rather than on the cellular membrane, as observed in high-grade non-ECM3 tumors. Scale bars, 100 μm.

(E) Quantitative IHC data showing the percentage of Twist-positive nuclei and the intensity score of β-catenin staining in 11 high-grade ECM3 tumors and 15 high-grade non-ECM3 tumors (***$p < 0.001$, ****$p < 0.0001$; Mann-Whitney *U* test). Single values are shown; bar indicates mean ± SEM.

(F) Representative IHC analysis of SPARC expression in high-grade ECM3 and non-ECM3 tumors. Scale bars, 100 μm.

(G) Quantitative IHC data showing the intensity score for SPARC in tumor and stromal cells of 11 high-grade ECM3 tumors and 15 high-grade non-ECM3 tumors (**$p < 0.01$, ****$p < 0.0001$; Mann-Whitney *U* test). Single values are shown; bar indicates mean ± SEM.

(H) Representative IHC analysis of $CD33^+$ cells infiltrating high-grade ECM3 and non-ECM3 tumors. Scale bars, 100 μm.

(I) Quantification of $CD33^+$ cells in 11 high-grade ECM3 and 15 high-grade non-ECM3 tumors (***$p < 0.001$; Mann-Whitney *U* test). Single values are shown; bar indicates mean ± SEM.

For additional data, see Figure S1 and Tables S1 and S2.

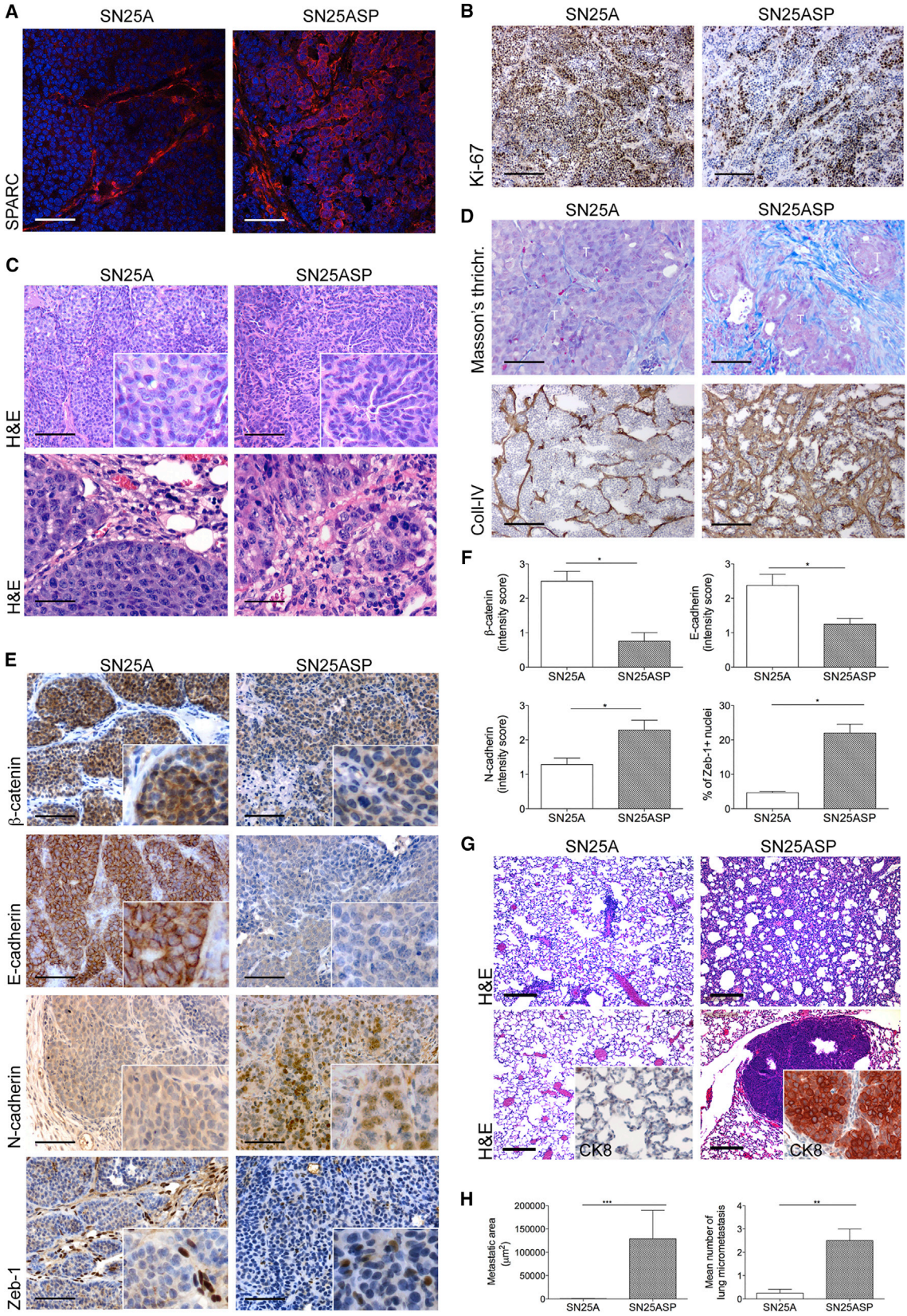

(legend on next page)

cells with a monocytoid morphology dispersed within stroma bundles (Figures 1H, 1I, and S1B; Table S2). This finding suggests that the different ECM characteristics of high-grade breast cancers lay the basis for a direct interaction between the tumor and myeloid cells and eventually affects the EMT features.

SPARC-Overexpressing Cells Undergo Epithelial-to-Mesenchymal Transition In Vivo, but Not In Vitro

To functionally link SPARC expression in cancer cells with tumor-myeloid cell contact and gaining of EMT phenotype, we developed ad hoc murine models consisting of SPARC-deficient (SN25A) or low-SPARC-expressing (N3D) breast cancer cell lines and their SPARC-transduced isogenic counterparts (SN25ASP and N3DSP). The parental and SPARC-transduced cells injected into syngeneic BALB/c mice mimicked non-ECM3 and ECM3 high-grade carcinomas, showing SPARC expression confined to stroma cell components or extending to tumor clones, as exemplified by SN25A and SN25ASP, respectively (Figure 2A). In vivo, SPARC-transduced tumors showed a reduction of both tumor growth (Figure S2) and proliferative index (Ki-67 staining) (Figures 2B and S2) compared to SPARC null (SN25A) tumors. Histological and immunohistochemistry (IHC) analysis of H&E-stained SN25ASP tumors showed the presence of cells with a spindle-like morphology intermingled with abundant collagen and forming ill-defined nest-like structures, a characteristic typical of cancers undergoing EMT (Figures 2C and 2D**)**. Additionally, the stromal septa were interrupted and unable to form defined lobular structures (Figures 2C and 2D**)**. Indeed, SN25ASP tumors displayed more evident infiltrative growth and better integration within the surrounding stroma (Figures 2C and 2D). In sharp contrast, parental SN25A tumors were characterized by epithelial cells organized in lobular structures with regular contours embedded in a dense stroma (Figures 2C and 2D**)**. The histopathological results were supported by fluorescence-activated cell sorting (FACS) analysis showing decreased E-cadherin expression and increased N-cadherin expression in a fraction of the cells deriving from SN25ASP tumors (Figure S2). A more in-depth IHC analysis, extended to other markers, showed upregulation and nuclear localization of N-cadherin and Zeb-1 as well as a downregulation of β-catenin and E-cadherin (see Figures 2E and 2F and Table S3 for cumulative data), which also showed a cytoplasmic to nuclear relocalization in some areas of SN25ASP tumors. The presence of metastasis in lungs from SN25ASP (but not SN25A) tumor-bearing mice confirmed the more aggressive phenotype of SN25ASP tumors (Figures 2G and 2H).

The lack of differences in E-cadherin and N-cadherin expression in all the cell lines in vitro (Figure S2) suggested that SPARC-induced EMT is not cell autonomous but requires contributions from other cells in the microenvironment, which, according to the patient data, could be of myeloid origin.

In situ immunostaining of Gr-1 and Ly6C markers showed that SN25ASP tumors exhibited more Gr-1^{+} and Ly6C^{+} myeloid cell infiltration than the parental SN25A tumors (Figures 3A and 3B). Cells with this phenotype belong to the so-called myeloid-derived suppressor cell (MDSC) populations that can be subdivided, by FACS analysis, into two canonical subsets: the granulocytic (G-MDSCs) (CD11b^{+}Gr-1^{high}Ly6C^{low}) and monocytic (M-MDSCs) subsets (CD11b^{+}Gr-1^{low}Ly6C^{high}) (see Figure S2 for the gating strategy) (Gabrilovich et al., 2012). In accordance to the IHC data, FACS analysis confirms that SN25ASP tumors contain more myeloid cells of both subsets (Figure 3C). Similar to their high-SPARC ECM3 human breast counterparts (Figure 1B), myeloid cells were closely associated with cancer cells in SN25ASP tumors (Figure S2). Additionally, similarly to what had been observed in human non-ECM3 tumors, SN25A tumors showed few myeloid cells, mainly localized within the stroma, surrounding cancerous epithelial nests (Figures 3A and S2).

Collectively, these results indicate that sustained SPARC expression in cancer cells promotes EMT and tumor aggressiveness in vivo.

To validate the above results in another tumor cell line, the BALB-NeuT transgenic-derived N3D cell line, chosen on the basis of its low expression of SPARC (Sangaletti et al., 2003), was rendered high SPARC expressing through retroviral gene transduction. SPARC overexpression affected poorly or not at all the in vivo growth and proliferation of tumors (Figure S3), as observed for the SN25A and SN25ASP pair, while it induced EMT. Indeed, the transduction of SPARC in N3D cells promoted a shift toward a spindle-shape morphology with an increased collagen content (Figure S3). IHC analysis showed the upregulation of N-cadherin and Zeb-1 together with the downregulation

Figure 2. SPARC Expression in Cancer Cells Promotes EMT and Tumor Aggressiveness In Vivo

(A) Immunofluorescence analysis of SPARC expression in SN25A and SN25ASP tumors. Scale bars, 50 μm.

(B) Representative IHC analysis of the Ki-67 marker in SN25A and SN25ASP tumor sections (cumulative data are shown in Figure S2B). Scale bars, 200 μm.

(C) H&E analysis of SN25A and SN25ASP tumors showing the presence of cells with a mesenchymal, spindle-like morphology in SN25ASP tumors. SN25ASP tumors also displayed more evident infiltrative growth with better integration within the surrounding stroma. Scale bars represent 200 μm (top) and 50 μm (bottom).

(D) Collagen deposition in SN25A and SN25ASP tumors evaluated using Masson's trichrome staining (scale bars, 100 μm) and IHC for collagen type IV (scale bars, 200 μm). Both analyses highlight the increased collagen deposition characteristic of SN25ASP tumors compared with their SN25A counterparts.

(E) IHC analysis of epithelial (β-catenin and E-cadherin) and mesenchymal (N-cadherin and Zeb-1) markers performed in SN25A and SN25ASP tumors. Scale bars, 100 μm.

(F) Quantitative IHC data for the EMT are shown as the intensity score in the case of β-catenin, E-cadherin, and N-cadherin or as the fraction of positive nuclei in case of Zeb1 (*$p < 0.05$, n = 10 cases per tumor type; Mann-Whitney *U* test).

(G) Representative H&E analysis of lungs from SN25A and SN25ASP tumor-bearing mice showing the increase in overall cellularity (upper panels) or micrometastases (lower panels) (CK8^{+}, inset) in the case of SN25ASP bearers. Scale bars, 200 μm.

(H) Quantitative data on micrometastases were obtained by measuring the size and the number of micrometastases (LasV program, Leica Microsystems; **$p < 0.01$, ***$p < 0.0001$; n = 10 cases per tumor type, Mann-Whitney *U* test).

Graphs show mean values plus SEM (upper bar). For additional data, see Figures S2–S4 and Table S3.

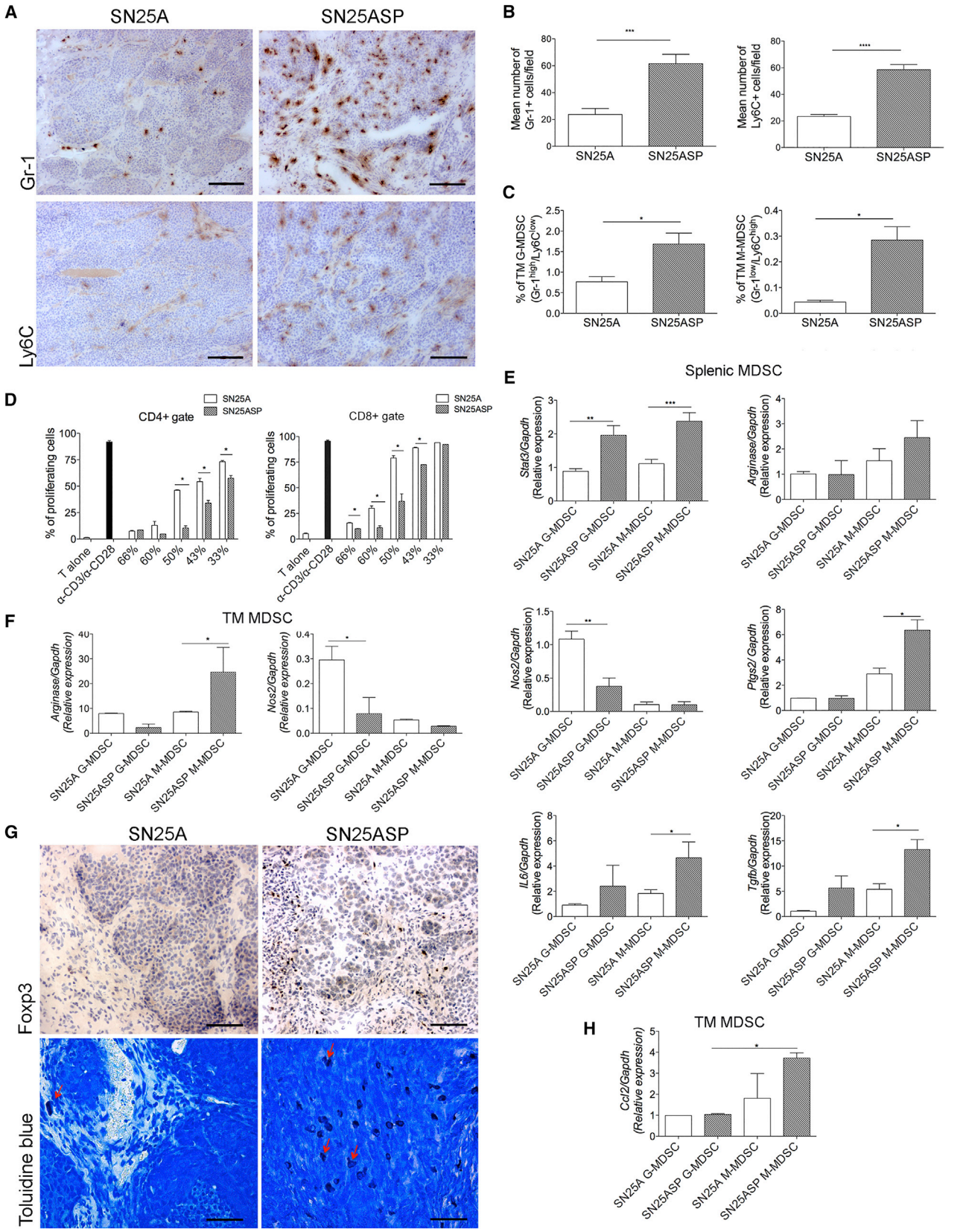

(legend on next page)

of β-catenin and E-cadherin, compatible with a shift toward a mesenchymal cell phenotype (Figure S3); notably, the phenotype of the N3DSP tumors showed reduced EMT and less aggressiveness compared to SN25ASP (Figure S4), most likely because of reduced expression of SPARC. Moreover, the N3DSP tumor-bearing mice showed diffuse lung colonization, which never induced solid tumor masses (Figure S4).

In situ immunostaining and FACS analysis of Gr-1 and Ly6C markers confirmed that SPARC overexpression induced more Gr-1$^+$ and Ly6C$^+$ myeloid cell infiltration in N3DSP than in its N3D counterpart (Figure S4).

SPARC Expression in Cancer Cells Affects Myeloid Cell Expansion and Function

Myeloid cells have been associated with tumor growth and metastasis and, more recently, with the EMT (Toh et al., 2011). We have previously shown that SPARC produced by mesenchymal cells affects myeloid cell precursors within normal BM niches (Tripodo et al., 2012), suggesting that SPARC and mesenchymal and myeloid cell characteristics could be linked in the cancer microenvironment. The injection of transplantable murine breast carcinoma cells into mice produces a marked leukemoid reaction, which is a myeloproliferative response characterized by the expansion of myeloid cells and relative precursors in hematopoietic organs (Wilcox, 2010). We evaluated the expansion of myeloid cells (CD11b$^+$, G-MDSCs and M-MDSCs) in the BM, spleen, and peripheral blood (PB) of SN25A and SN25ASP tumor-bearing mice. Both types of tumors induced the expansion of myeloid cells in all analyzed compartments (see Figure S5 for quantitative data and gating parameters), with some differences in progeny maturation being observed, as SN25ASP tumors were more efficient in expanding monocytic myeloid cells in the PB (Figure S5). This difference is even more relevant considering the generally reduced tumor burden of SN25ASP tumors and suggests that this type of tumor induces myeloid cell expansion more efficiently than its SN25A counterpart. In line with the tumor-associated immunosuppression activity attributed to tumor-induced myeloid cells, we compared the ability of spleen-derived myeloid cells from mice bearing SN25A and SN25ASP tumors to suppress α-CD3- and α-CD28-induced T cell proliferation. Results showed that the whole CD11b$^+$Gr-1$^+$ myeloid cells (comprising both MDSC subsets) isolated from SN25ASP tumor-bearing mice, according to Melani and co-workers (Melani et al., 2003), suppressed T cell proliferation more efficiently than those from SN25A tumor-bearing mice (Figure 3D). The above findings were confirmed with the N3D model, in which SPARC overexpression promoted the expansion of myeloid cells in the spleen and PB (Figure S6), and resulted in a more suppressive phenotype (Figure S6).

The two G-MDSC and M-MDSC subsets were obtained from the spleens of mice bearing SN25A or SN25ASP tumors through cell sorting and then analyzed through semiquantitative real-time PCR to determine the expression of key MDSC genes, including *Stat3*, *Arginase1*, *Nos2*, *Ptgs2*, *IL6*, and *Tgfb1*. Splenic myeloid cells isolated from SN25ASP-bearing mice expressed higher levels of *Stat3*, *IL6*, and *Tgfb1*, which is the master inducer of MDSCs. *Arginase1* was barely detectable in the splenic myeloid cell subsets, and it was therefore not possible to assess significant differences between the groups (Figure 3E). However, when *Arginase1* was evaluated in tumor-associated myeloid cells, it was found to be expressed at a significantly higher level in M-MDSCs from SN25ASP tumors than in those from SN25A tumors (Figure 3F). In contrast to the other MDSC markers, *Nos2* was reduced in both tumor and splenic suppressive MDSC isolated from SN25ASP-bearing mice (Figures 3E and 3F). Nevertheless, NOS2 is known for its dual function, and it is also expressed in inflammatory M1-type myeloid cells (Mantovani et al., 2002).

Because myeloid cells interact and co-exist with regulatory T cells (Huang et al., 2006), B cells, and mast cells (MCs) (Danelli et al., 2015), to generate an immunosuppressive microenvironment, we also evaluated whether variations in myeloid cells were associated with changes in other immune cell populations within tumors. IHC analysis of SN25ASP showed enrichment in Foxp3$^+$ regulatory T (Treg) cells (Figures 3G and S6), increased MC recruitment (Figures 3G and S6) and inversion of the T/B lymphocyte ratio in favor of B cells (Figure S6). The recruitment of immunosuppressive cells could be explained by the increased expression of CCL-2 by intra-tumor MDSCs in SN25ASP

Figure 3. SPARC Expression in Cancer Cells Affects the Expansion, Recruitment, and Function of Myeloid Cells

(A) IHC analysis of the myeloid markers Gr-1 and Ly6C performed on SN25A and SN25ASP tumors, showing enrichment in myeloid cells and close proximity to tumor cells in SN25ASP tumors. Scale bars, 100 μm.

(B) Quantitative IHC data for Gr-1and Ly6C were obtained by counting the number of Gr-1$^+$ or Ly6C$^+$ cells in five fields from ten SN25A and ten SN25ASP tumors (***p < 0.001, ****p < 0.0001; Mann-Whitney *U* test).

(C) FACS analysis of G- and M-MDSCs performed on fresh tumors isolated from ten SN25A and ten SN25ASP-bearing mice (*p < 0.05, ***p < 0.0001; Mann-Whitney *U* test).

(D) Immunosuppressive activity of CD11b$^+$Gr-1$^+$ myeloid cells isolated from the spleens of SN25A and SN25ASP tumor-bearing mice evaluated as the ability to suppress α-CD3/α-CD28-induced CD4 and CD8 T cell proliferation in vitro (one of three representative experiments performed with similar results). The multiple Student t test was used for statistical analysis (*p < 0.05).

(E) Semiquantitative real-time PCR analysis of the *Stat3*, *Nos2*, *Arginase1*, *Ptgs2*, *IL6*, and *Tgfb1* genes was performed on the G-MDSC and M-MDSC subsets sorted from the spleens of SN25A and SN25SP tumor-bearing mice (n = 5 per subset of MDSCs). The Mann-Whitney *U* test was used for statistical analysis (*p < 0.05; **p < 0.01; ***p < 0.001).

(F) Semiquantitative real-time PCR analysis of *Arginase1* and *Nos2* was performed on the G-MDSC and M-MDSC subsets sorted from SN25A and SN25SP tumors (n = 3/subset of MDSCs, n = 3/tumors; each sample represents a group of three mice). The Student's t test was used for statistical analysis (*p < 0.05).

(G) Top: representative IHC analysis of Foxp3$^+$ cells in SN25A and SN25ASP tumors (quantitative IHC data are shown in Figure S5). Scale bars, 100 μm. Bottom: toluidine blue staining highlighting mast cell infiltration in SN25A and SN25ASP tumors (quantitative IHC data are shown in Figure S5). Scale bars, 50 μm.

(H) Semiquantitative RT-PCR analysis of *Ccl2* genes performed on G- and M-MDSCs isolated from SN25A and SN25ASP tumors (n = 3/tumors, each sample represents a group of three mice). The Student's t test was used for statistical analysis (*p < 0.05).

Graphs show mean value plus SEM (upper bar). For additional data, see Figures S5 and S6.

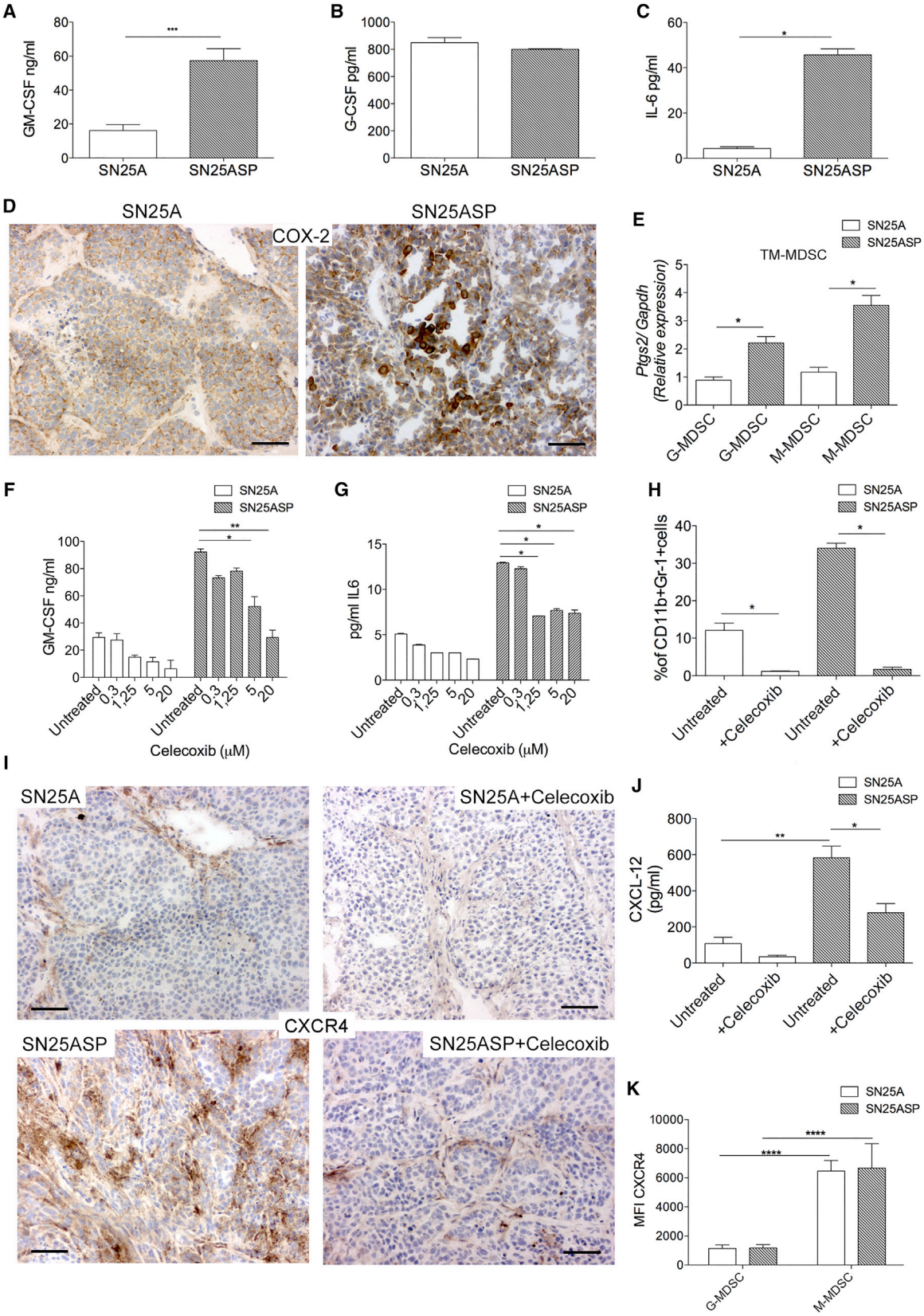

(legend on next page)

tumor-bearing mice (Figure 3H), as CCL-2 is a chemo-attractant for both Treg cells and MCs (Collington et al., 2010). Further confirming the increase of local immunosuppression, the microenvironment of SN25ASP tumors was rich in interleukin-10 (IL-10), a prototypical immunosuppressive cytokine (Figure S6). Similar findings were obtained using the N3D/N3DSP pair in which SPARC overexpression increased MC and Foxp3$^+$ cell infiltration (data not shown).

These data indicate that cancers characterized by high endogenous SPARC expression can generate an immunosuppressive microenvironment mainly through the action of MDSCs.

Tumor-Derived SPARC Promotes GM-CSF and IL-6 Production via COX-2

The mechanism underlying the tumor-intrinsic SPARC modulation of tumor-associated myeloid cell phenotypes was investigated, considering that myeloid cell polarization is chiefly influenced by granulocyte-macrophage colony-stimulating factor (GM-CSF). GM-CSF, which is expressed at different levels in various tumor types, is one of the main inducers of tumor-associated myelopoiesis and, together with IL-6, is responsible for the expansion of MDSCs (Marigo et al., 2010). Thus, we evaluated GM-CSF levels in 48-hr supernatants from SN25A and SN25ASP tumor cell lines and observed a higher production in the latter cell line (Figure 4A). Additionally, IL-6 production was higher in SN25ASP cells than their wild-type (WT) counterparts, whereas granulocyte colony-stimulating factor (G-CSF) was produced in equal amounts (Figures 4B and 4C). The link between SPARC and GM-CSF production is thought to depend on COX-2, an enzyme that is co-regulated with SPARC, in various pathological settings (Said et al., 2007) and plays a key role in tumor immunosuppression (Rodriguez et al., 2005). SPARC regulation of fibrillar collagens (Sangaletti et al., 2003) can in turn modulate COX-2 expression (Lyons et al., 2011). Indeed, in models of pregnancy-associated breast cancer, non-steroidal anti-inflammatory drug (NSAID) treatment inhibits tumor progression, suppressing COX-2-dependent collagen deposition (Alique et al., 2011).

IHC evaluation of SN25ASP tumors showed that, consistent with a tight ECM (Figure 2), the expression of COX-2 was high both in tumor cells and in infiltrating myeloid cells (Figure 4D). In particular, qPCR analysis confirmed that MDSC isolated from SN25ASP tumors, but not SN25A tumors, expressed higher COX-2 gene (*Ptgs2*) levels (Figure 4E), confirming their suppressive activity as reported in splenic MDSCs.

To test whether the increased production of GM-CSF and IL-6 depends on COX-2 activity in SN25ASP tumor cells, cells were treated with the COX-2-specific inhibitor celecoxib for 48 hr, and cell supernatants were subsequently analyzed via ELISA. The treatment significantly reduced not only GM-CSF but also IL-6 production (Figures 4F and 4G), without affecting G-CSF. These results indicate that COX-2 activity regulates the balance between G-CSF and GM-CSF in SPARC-rich tumors, stimulating GM-CSF and promoting the environmental immunosuppression by upregulating IL-6 secretion. In addition, these tumors are locally enriched in infiltrating myeloid cells, whose recruitment might depend on COX-2 (Obermajer et al., 2011). Notably, the high chemotactic activity of SN25ASP in myeloid cell recruitment, measured using a transwell-based migration assay, was abrogated by the addition of celecoxib (Figure 4H). The pathway controlled by COX-2 was found to be relevant also in vivo, where celecoxib reduced the recruitment of CXCR4$^+$ infiltrating cells (Figure 4I) via downregulation of CXCL12, which is highly expressed in SN25ASP tumors. Furthermore, ELISAs performed on sera from SN25A and SN25ASP tumor-bearing mice showed higher CXCL12 levels in SN25ASP bearers and a decrease of this chemokine upon celecoxib treatment in vivo (Figure 4J). This decrease in CXCR4$^+$ myeloid cell infiltration was not determined by a different surface expression of CXCR4, which was similar in circulating MDSCs from SN25A and SN25ASP-bearing mice (Figure 4K).

These data correlate with human cases of high-grade ECM3 tumors that display increased COX-2 expression in both tumor and stromal cells compared to non-ECM3 tumors (Figure 5; Table S2).

Targeting the Suppressive Subset of Myeloid Cells Improves the Outcome of Chemotherapy in EMT Tumors

To determine whether myeloid cells with immunosuppressive properties are a limiting partner in the EMT, the activity of these

Figure 4. Tumor-Derived SPARC Promotes GM-CSF and IL-6 Production as well as CXCR4$^+$ Cell Recruitment via COX-2

(A–C) Production of G-CSF, GM-CSF, and IL-6 in the 48-hr supernatants of SN25A and SN25ASP cell lines in vitro, quantified through specific ELISAs (n = 5/cell line; *p < 0.05; ***p < 0.001; Mann-Whitney *U* test).

(D) IHC analysis of COX-2 expression performed on SN25A and SN25ASP tumors showing increased production of COX2 by both tumor cells (black arrows) and infiltrating myeloid cells (white arrows) in SN25ASP tumors. Scale bars, 100 μm.

(E) Semiquantitative real-time PCR analysis of *Ptgs2* performed on G- and M-MDSCs sorted from SN25A and SN25ASP tumors (n = 3/subset of MDSCs; each subset represents a group of three mice; *p < 0.05; Student's t test).

(F and G) Production of GM-CSF and IL-6 in 48-hr supernatants of SN25A and SN25ASP tumors treated with or without scalar doses of the COX-2 inhibitor celecoxib (one of two representative experiments performed with similar results). The Student's t test was used for statistical analysis (*p < 0.05; **p < 0.01).

(H) Cumulative data showing the percentage of CD11b$^+$Gr-1$^+$ cells that migrated toward SN25A and SN25ASP tumors (one out of two representative experiments performed with similar results). The Mann-Whitney *U* test was used for statistical analysis (*p < 0.05).

(I) IHC analysis of CXCR4 expression in SN25A and SN25ASP tumors upon celecoxib treatment in vivo (for quantitative data, see also Figure S5). Scale bars, 100 μm.

(J) Serum level of CXC12 in mice bearing SN25A or SN25ASP tumors and treated with celecoxib (n = 5/tumor type/treatment; statistical analysis by Mann-Whitney *U* test: *p < 0.05; **p < 0.01).

(K) PB FACS analysis showing the expression of CXCR4, evaluated as the mean fluorescence intensity (MFI), in G- and M-MDSCs from SN25A- and SN25ASP-bearing mice. The Mann-Whitney *U* test was used for statistical analysis (****p < 0.0001; n = 5/tumor type).

Graphs show mean value plus SEM (upper bar).

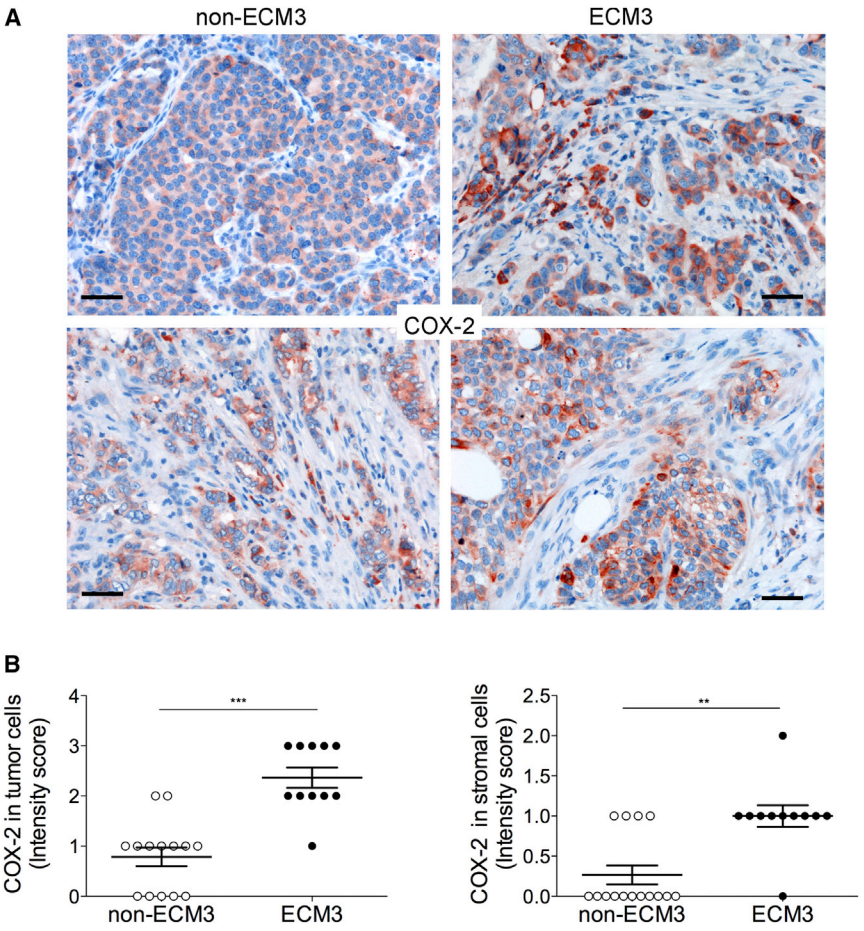

Figure 5. Differential COX-2 Expression in ECM3 and Non-ECM3 Tumors

(A) IHC analysis of COX-2 expression in two representative high-grade ECM3 and non-ECM3 tumors. Scale bars, 50 μm.

(B) Quantitative IHC data showing the intensity score for COX-2 in tumor and stromal cells of 11 ECM and 15 non-ECM 3 high-grade tumors (**$p < 0.01$; ***$p < 0.001$, Mann-Whitney *U* test). Single values are shown; bar indicates mean ± SEM. For additional data, see Table S2.

cells was targeted using aminobisphosphonates (zoledronic acid [ZA]), which we had previously shown to reduce tumor-induced immune suppression in transgenic p185/HER-2 mice (Melani et al., 2007). Mice bearing SN25ASP tumors 8 mm^3 in size were treated daily with ZA (0.1 mg/kg). Three weeks later, mice were sacrificed and their tumors were histologically analyzed. ZA treatment did not significantly reduce tumor growth; however, histological and IHC analyses showed a reversion of the EMT phenotype in vivo (see Figures 6A–6D and Table S3 for cumulative data). To investigate the correlation between the EMT reversion and the changes in the suppressive function of MDSCs, we performed a semiquantitative PCR analysis of suppressive markers on myeloid cells isolated from the spleens (*Stat3*, *TGFbeta*) or tumors (*Arg1*, *CCL2*) of ZA-treated mice and tested their suppressive activity in vitro. Results showed a significant down-modulation of *Stat3*, *Arginase1*, *Tgfb1*, and *Ccl2* in both the G- and M-MDSC subsets (Figure 6E). Moreover, ZA treatment abrogated the capacity of myeloid cells ($CD11b^+Gr\text{-}1^+$) to suppress T cell proliferation (Figure 6F). These data indicate that ZA treatment reverts the suppressive phenotype of MDSCs and their activity in promoting the EMT.

As a consequence of the reduction of EMT, treatment with ZA increased the Ki-67 proliferation index (Figures 7A and 7B) in SN25ASP tumors. This finding could be clinically relevant, considering that DNA-intercalating drugs exhibit poor activity in quiescent cells, and was therefore investigated in mice bearing SN25ASP and SN25A tumors. Mice bearing tumors of nearly 8 mm^3 in size were randomized in four groups, which received the following treatments: (1) Doxil, a pegylated non-cardiotoxic form of doxorubicin (10 mg/kg once a week); (2) ZA; (3) a combination of Doxil and ZA; and (4) saline, as a control. Although SN25ASP tumors were less sensitive to Doxil treatment than SN25A (Figures 7C–7G), in accordance to their EMT status and low proliferation rate (Figure 2), the addition of ZA rendered SN25ASP and SN25A tumors equally sensitive to treatment (Figures 7C–7G). These data indicate that the detrimental effect of MDSCs on immune function and the EMT can be reverted using ZA. Notably, ZA treatment also reduced lung metastasis, particularly in combination with Doxil (Figures 7H–7J). Finally, as with ZA treatment, the COX-2 inhibitor celecoxib showed an additive effect together with Doxil in reducing the tumor volume (Figure S7); however, it mainly affected the recruitment of MDSCs (Figure S7) rather than their suppressive function (data not shown). Notably, celecoxib-treated tumors showed fewer $Zeb\text{-}1^+$ nuclei and increased β-catenin expression suggestive of reduced EMT features (see Figure S7 and Table S3 for cumulative data).

DISCUSSION

In this study, we have shown that the matricellular protein SPARC is involved in the dynamics linking MDSCs and breast cancer cells toward EMT.

In solid cancers, the degree of EMT correlates with tumor aggressiveness. Breast cancers can vary the composition of the associated ECM, together with their EMT status. In this context, two breast cancer prognostic groups (ECM3 and non-ECM3) were defined on the basis of specific ECM signatures (Triulzi et al., 2013). Of note, *Sparc* was the leading gene of the ECM3 signature marking high-grade tumors with EMT characteristics and poor response to therapy.

Here, we have shown that high-grade human breast cancers with a *Sparc*-high ECM signature expressed SPARC in both

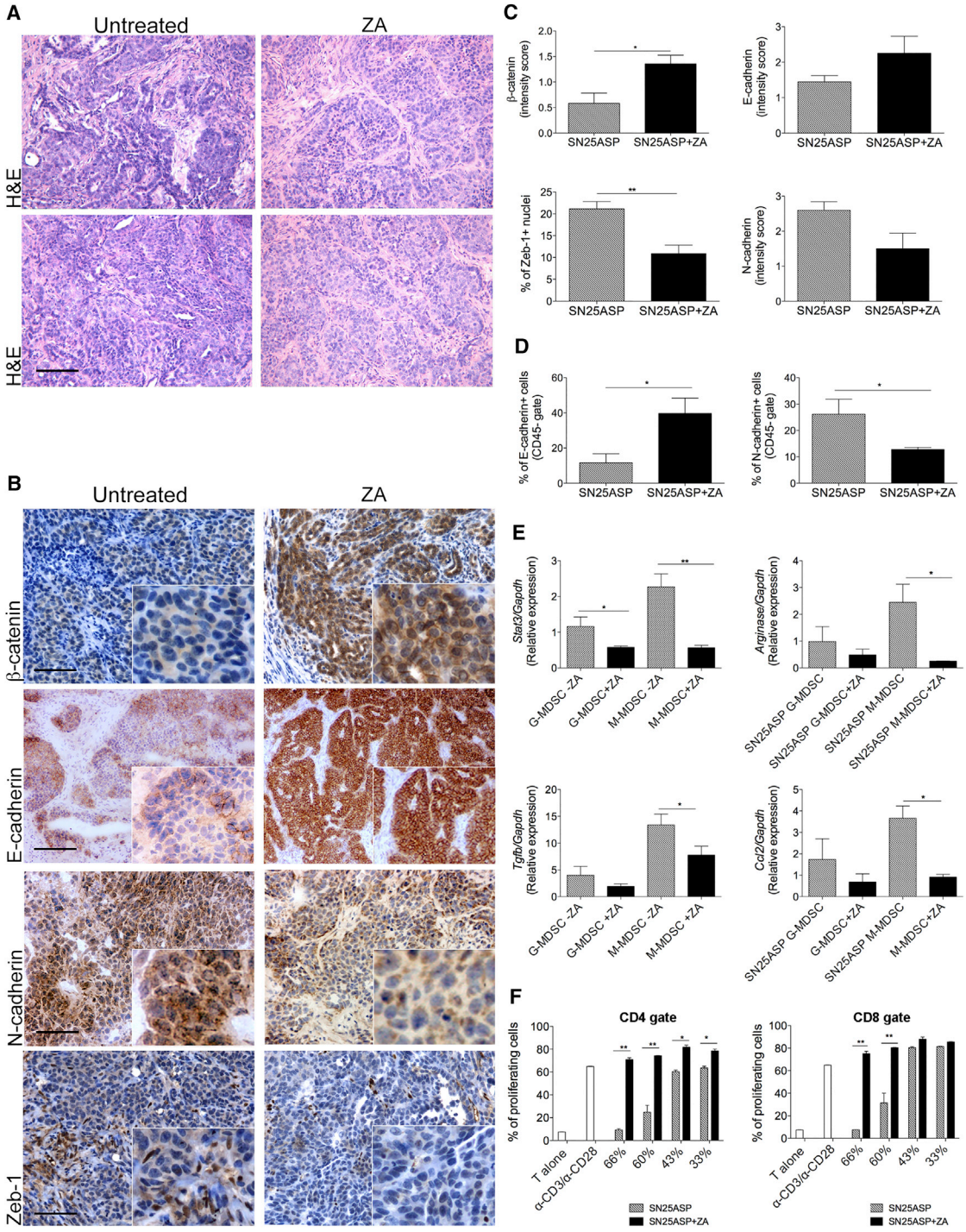

Figure 6. Targeting the Suppressive Subset of Myeloid Cells Reverts the EMT Phenotype

(A) Histological analysis of two representative controls and ZA-treated SN25ASP tumors showing a reduction in cells with a mesenchymal, spindle-like morphology in tumors from ZA-treated mice. Scale bars, 200 μm.

(B) Representative IHC analysis of epithelial (β-catenin and E-cadherin) and mesenchymal (N-cadherin and Zeb-1) markers, performed on SN25ASP tumors treated with or without ZA. Scale bars, 100 μm.

(C) Quantitative IHC data for EMT markers are shown as intensity scores in the case of β-catenin, E-cadherin, and N-cadherin or as the fraction of positive nuclei in the case of Zeb-1 (*$p < 0.05$; **$p < 0.01$; $n = 10$ case/treatment; Mann-Whitney *U* test). Additional data are shown in Table S3.

(legend continued on next page)

tumor cells and stroma, a combination that was associated with evident EMT features. In clear contrast, high-grade tumors in which SPARC was confined to the stroma exhibited a lower degree of EMT. An important distinction between ECM3 and non-ECM3 cancers, together with SPARC immunolocalization, derived from the homing of immature $CD33^+$ myeloid elements. These cells were in close contact with tumor cells expressing high levels of SPARC while remaining confined within the mesenchymal cell axes when SPARC production was limited to the stroma. This finding suggested a complex interplay between the ECM properties and myeloid cells in determining the EMT phenotype. Indeed, EMT can result from either cancer cell-intrinsic molecular programs (Yang et al., 2004) or pressure from the microenvironment (Reiman et al., 2010).

In this work, we demonstrate that the microenvironmental induction of EMT depends on SPARC regulation of the interplay between MDSCs and ECM. Indeed, SPARC produced by tumor cells promoted the expansion and recruitment of the immunosuppressive myeloid cells that were necessary for EMT. High-SPARC tumors were characterized by abundant collagen bundles, which have been shown to induce the expression of COX-2 in the mammary epithelium (Lyons et al., 2011). In turn COX-2 induced GM-CSF and IL-6 expression, which explained the preferential expansion of myeloid cells with suppressive activity (Marigo et al., 2010). In addition, COX-2 activation of the CXCL12-CXCR4 axis promoted the recruitment of myeloid cells to the tumor site. Accordingly, a COX-2 inhibitor (celecoxib) was able to block the migration of myeloid cells to SPARC-producing tumors.

To study the role of myeloid cells in the EMT, mice were treated with ZA, a type of drug that is capable of interfering with MDSC expansion (Melani et al., 2007) and differentiation. We showed that ZA inhibited the suppressive activity of MDSCs and, in turn, reverted EMT. This proves that MDSC activity was required to maintain a non-cell-autonomous EMT. This is in clear agreement with what we observed in celecoxib-treated tumors that displayed reduced EMT features because of diminished intra-tumor accumulation of MDSCs.

High-grade ECM3 human breast cancers are generally resistant to chemotherapy. Our experimental model suggests that the combination of cytotoxic agents with ZA (or celecoxib) can revert chemoresistance in this particular ECM setting. Discordant data exist concerning whether the adjuvant use of ZA might be effective in ameliorating the outcome of breast cancer patients. Strikingly, both an increased overall survival (Diel et al., 1998) and an absence of activity (Saarto et al., 2004); (Kristensen et al., 2008) have been reported. A study involving 1,803 premenopausal women with estrogen-receptor-positive breast cancer showed a reduced risk of disease recurrence (Gnant et al., 2009). On the contrary, a larger study, involving 3,360 patients, showed no increase in overall survival or change in the rate of invasive disease-free survival when ZA was added to standard adjuvant therapy (Coleman et al., 2011).

In the light of our results, ZA treatment could be effective in cases where the interplay between immune cells and the tumor-associated ECM determines a progressive EMT phenotype. For example, ZA treatment could be exploitable in the treatment of high-grade ECM3 tumors (Triulzi et al., 2013) or low-claudin triple-negative breast tumors showing a concomitant enrichment in EMT and immune cell genes (Perou, 2010; Taube et al., 2010). Here, we describe a novel level of regulation of tumor EMT based on the interplay between tumor-associated ECM and MDSCs, presenting new immunomodulatory approaches. Our model is in line with the emerging relevance of the immune landscape of human tumors, to which it adds the ECM as a further determinant.

EXPERIMENTAL PROCEDURES

Patient Samples and Gene Expression Data

Consecutive primary breast tumors (97 cases) were surgically resected at Fondazione IRCCS Istituto Nazionale Tumori (Huang et al., 2015). The study was approved by the medical ethics committee, and all clinical data and tissue samples were obtained after receiving informed consent, according to institutional rules.

GSEA to assess the ECM, grade, and immune function associations of breast samples was performed using GSEAv2.2.0 (Subramanian et al., 2005) and a previously described cancer-related gene set database (Triulzi et al., 2013). Genes represented by more than one probe were collapsed to the probe with the maximum value using the collapse dataset tool. The gene set permutation type was applied 1,000 times. The enrichment score represents the degree to which each gene set is overrepresented at the top or bottom of the ranked list of genes in the expression dataset; the normalized enrichment score (NES) estimates the enrichment score after it has been normalized across analyzed gene sets; the NOM p value estimates the statistical significance of the enrichment score for a single gene set; the false discovery rate (FDR) q-value is adjusted for the size of the gene set and multiple hypothesis testing. A gene set was considered significantly enriched at nominal p value < 0.05 and FDR q-value < 0.20.

Animals and Cell Lines

BALB/cAnNCrl mice (BALB/c) were purchased from Charles River Laboratories. All experiments involving animals described in this study were approved by the Ministry of Health (authorization number 03/2012). The primary breast carcinoma cell line SN25A was obtained from *Sparc*-deficient mice that spontaneously developed mammary tumors due to the expression of the rat oncogene HER2 transgene (BALB/c; SPARC < tm1Hwe > Tg(MMTV-Erbb2) NK1Mul/J), whereas the N3D cell line was derived from transgenic Her2/Neu mice (BALB/c-Tg(MMTV-Erbb2)NK1Mul/J). Both cell lines were infected with the retroviral vector LXSPARCSH (Sangaletti et al., 2011) and subjected to ectopic SPARC expression.

(D) FACS analysis of N-cadherin and E-cadherin performed on freshly isolated SN25ASP tumors treated with or without ZA. FACS analysis showed that ZA treatment increases the fraction of E-cadherin-positive cells while decreasing that of N-cadherin-positive cells in SN25ASP-treated tumors (*p < 0.05; Mann-Whitney *U* test).
(E) Semiquantitative real-time PCR analysis of *Stat3*, *Tgfb1*, *Arginase1*, and *Ccl2* was performed on the G-MDSC and M-MDSC subsets isolated from the spleens (*Stat3*, *Tgfb*) or tumors (*Arginase*, *CCL2*) of SN25SP tumor-bearing mice treated with ZA (n = 5/subset of MDSCs; *p < 0.05; **p < 0.01; Mann-Whitney *U* test).
(F) In vitro suppressive activity (day 3) of $CD11b^+Gr\text{-}1^+$ MDSCs isolated from the spleens of SN25ASP tumor-bearing mice treated or not with ZA. The samples were examined in triplicate. The experiment was performed three times, with overlapping results (*p < 0.05; **p < 0.01; multiple t test).
Graphs show mean value plus SEM (upper bar).

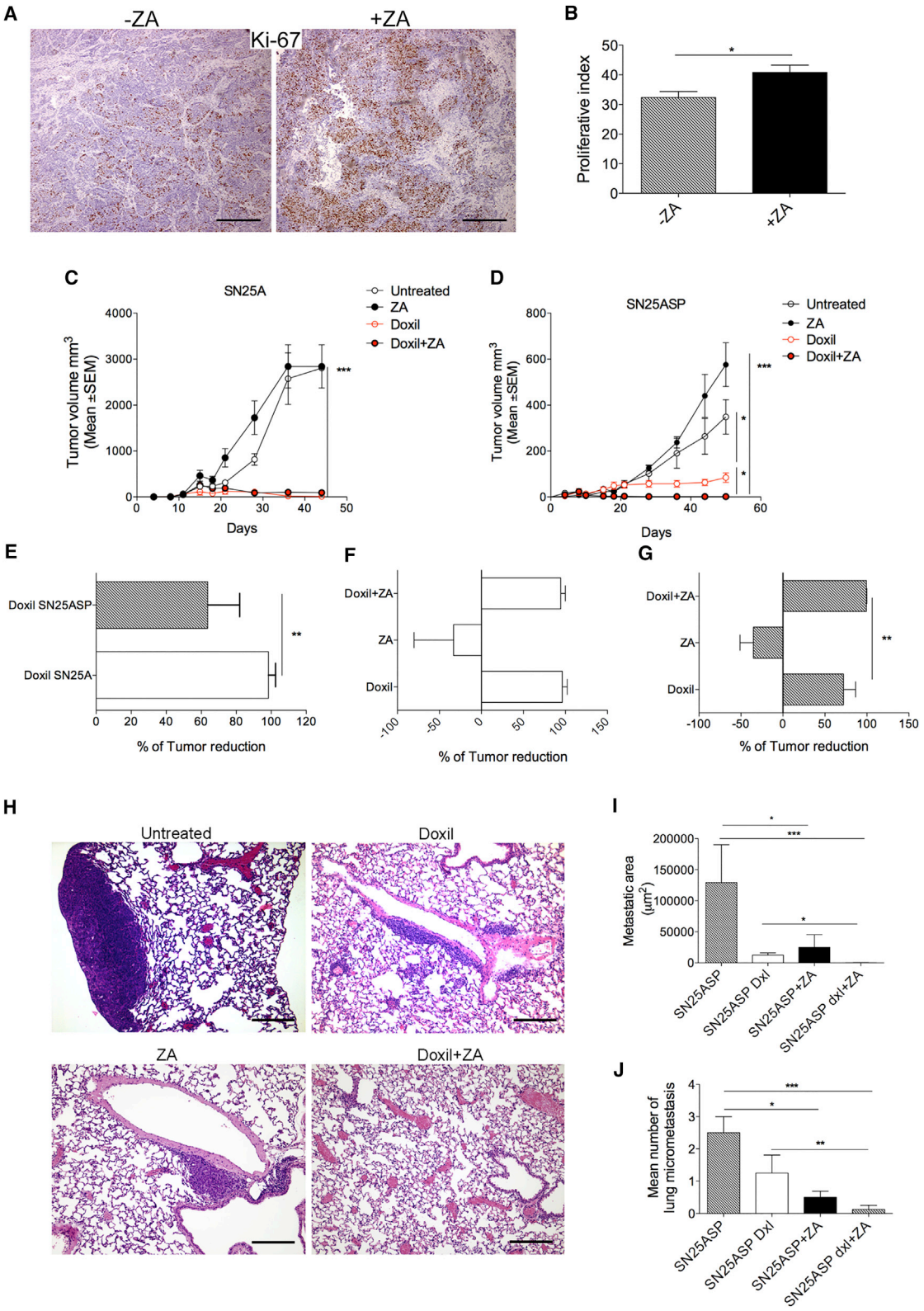

Figure 7. Targeting the Suppressive Function of Myeloid Cells Improves Chemotherapy

(A) IHC analysis of the Ki-67 proliferation marker performed on SN25ASP tumors treated with or without ZA. Scale bars, 200 μm.

(B) Proliferation index of SN25ASP tumors treated with or without ZA (n = 10/group; *p < 0.05; Mann-Whitney *U* test).

(legend continued on next page)

Treatments

Mice were subcutaneously injected with SN25A and SN25ASP tumor cells. When the tumors measured 8 mm^3, the mice were randomized into four different groups (ten mice per group) and treated with a pegylated form of doxorubicin (Doxil, Caelyx, 5 mg/kg once a week), ZA (Zometa, daily, 0.1 mg/kg) or celecoxib (5 mg/Kg, daily, ip), a combination of doxorubicin and ZA (or doxorubicin and celecoxib), or left untreated.

Isolation of Splenic MDSCs

G-MDSCs ($CD11b^+Gr\text{-}1^{high}Ly6C^{low}$) and M-MDSCs ($CD11b+Gr\text{-}1^{low}Ly6C^{high}$) were isolated from the spleens of tumor-bearing mice through immunomagnetic separation using a specific kit purchased from Miltenyi Biotec. The purity of the G-MDSC and M-MDSC populations was checked via FACS using the following antibodies: PerCP-CY5.5-conjugated anti-mouse CD11b (M1-70), fluorescein isothiocyanate (FITC)-conjugated anti-mouse Ly-6G (Gr-1) (RB6-8C5), and allophycocyanin (APC)-conjugated Ly6C anti-mouse (clone HK1.4). MDSCs obtained through immunomagnetic separation were used for real-time PCR analysis and suppression assays. Low-abundance tumor-derived MDSCs were obtained through cell sorting using a FACSAria cell sorter (BD Biosciences). The purity of the cell populations was >99%. Tumor tissues were cut into small pieces and treated with collagenase (type IV, 1 mg/mL, Sigma-Aldrich) and elastase (6 U/mL, Sigma-Aldrich) for 45 min at 37°C, and dead cells were then removed via centrifugation using a Ficoll-Hypaque gradient (Atlanta Biotechnology). Cell suspensions were stained with the following mixture of antibodies: PerCP-CY5.5-conjugated rat anti-mouse CD11b (M1-70), anti-mouse Ly-6G (Gr-1) FITC (clone RB6-8C5), and APC-conjugated rat anti-mouse Ly6C (clone HK1.4).

Suppression Assay

The suppression assay was performed as described previously (Sangaletti et al., 2014a). Briefly, 4×10^5 naive BALB/c splenocytes were labeled with carboxyfluorescein succinimidyl ester (CFSE; Sigma-Aldrich) and cocultured with $CD11b^+Gr\text{-}1^+$ myeloid cells at different ratios, in the presence of 2 μg/mL soluble anti-CD3 and 1 μg/mL anti-CD28 to activate lymphocytes. $CD11b\ (Mac\text{-}1)^+/Gr\text{-}1^+$ cells were isolated from spleen cells by means of CD11b-conjugated microbeads (Miltenyi) according to the manufacturer's instructions and as previously described (Melani et al., 2003). Each sample was seeded in triplicate. The proliferation of CD4 and CD8 T cells was assessed 2 and 3 days later through flow cytometry, evaluating CFSE dilution in the $CD4^+$- and $CD8^+$-gated populations. The results are shown as the percentage of proliferating cells.

Quantitative Real-Time PCR

For quantitative real-time PCR, myeloid cells were lysed with TRIzol (Invitrogen Life Technologies) and RNA was extracted using the RNeasy Kit (QIAGEN). DNA contaminants were removed by treatment with DNase I. cDNA was reverse transcripted from 1 μg total RNA. PCR was performed using TaqMan Universal PCR master mix (Applied Biosystems) and a target gene assay mix containing sequence-specific primers for the *Ccl2*, *Stat3*, *Arginase1*, *Nos2*, *Tgfb*, *IL6*, and *Ptgs2* genes. Gene-specific primers were purchased from Applied Biosystems (*Ccl2*, RefSeq NM_011333.3; *Stat3* NM_0114886.4; *Arginase1* NM_000036.2; *Nos2* NM_010927.3; *Tgfb1* NM_011577.2; *IL6* NM_ 031168.2; and *Ptgs2* NM_0111983). The reactions were set up according to the standard TaqMan qPCR conditions reported in the Applied Biosystems protocol and were performed in duplicate for each sample. The qPCR assays were run using the ABI PRISM 7900 Fast Real Time PCR system and the ABI PRISM 7900 HT Sequence Detection System (Applied Biosystems), and the resulting data were analyzed with SDS Software 2.3 (Applied Biosystems). The mRNA level of the target gene was quantified by measuring the CT value to determine its relative expression. The results are reported using the fold change in the gene expression of the target genes relative to the internal control gene (GAPDH). The mean-fold change in target gene expression was calculated as $2\text{-}\Delta\Delta CT$, where $\Delta\Delta CT$ = ((CT,Target − CT,GAPDH)sample-(CT,Target − CT,GAPDH)) internal control.

Histology and Immunohistochemistry

Histological and immunohistochemistry analyses of human and mouse tissues were performed as described previously (Tripodo et al., 2012), and details are provided in Supplemental Experimental Procedures.

ELISA Assay

To quantify GM-CSF, G-CSF, and IL-6 in supernatants, 10^6 SN25A and SN25ASP cells/mL were seeded in culture dishes. Cell-free supernatants were collected 48 hr later and then tested according to the manufacturer's instructions. The following kits were used: mouse IL-6 Quantikine ELISA (R&D Systems, M6000B), mouse G-CSF Quantikine ELISA (R&D, MCS00), and mouse GM-CSF ELISA Ready-SET-Go! (eBioscience, 88-7334-22). Serum level of CXCL12 was determined by using the mouse CXCL12 (SDF-1B) LEGEND MAX ELISA Kit (BioLegend, 444207) according to manufacturer's instructions.

Statistical Analysis

Statistical analysis of single treatments was performed using the Mann-Whitney *U* test. The significance of different combined treatments was assessed through one-way ANOVA with Dunn's multiple comparison test. For other analyses related to MDSC frequency or ELISA data, differences between groups were tested for significance using a two-tailed unpaired t test. Values were considered statistically significant when $p < 0.05$. All of the analyses were performed using Prism software Version 5.0d (GraphPad).

ACCESSION NUMBERS

The accession number for the gene expression data from the profiled samples reported in this paper is GEO: GSE59590.

SUPPLEMENTAL INFORMATION

Supplemental Information includes Supplemental Experimental Procedures, seven figures, and three tables and can be found with this article online at http://dx.doi.org/10.1016/j.celrep.2016.08.075.

AUTHOR CONTRIBUTIONS

S.S. and M.P.C. conceived the study, interpreted data, and designed the experiments. S.S., M.P.C. and C.T. wrote the manuscript. S.S., C.C., A.S., N.C., P.P., L.B., B.C., M.P., and A.G. performed the experiments and acquired data. S.S., C.C., and C.T. analyzed the data. R.O. analyzed GEP data. E.T., C.T., and

(C and D) Mean tumor volume of SN25A and SN25ASP tumors treated with Doxil or ZA, either as single agents or in combination. BALB/c mice were subcutaneously injected with SN25A and SN25ASP tumor cells. Once a tumor size of 8 mm^3 was reached, the mice were randomized into four different groups (seven mice per group) and treated with Doxil, ZA, a combination of Doxil and ZA, or left untreated. The representative experiment shows that SN25ASP tumors (D) were less sensitive to Doxil treatment and the sensitivity to this treatment was greatly improved when Doxil was administered in combination with ZA (*$p < 0.05$; ***$p < 0.0001$; Mann-Whitney *U* test; n = 10/treatment).

(E–G) Efficacy of Doxil or Doxil plus ZA treatment expressed as the percentage of tumor volume reduction for both cell lines (*$p < 0.05$; **$p < 0.01$; Mann-Whitney *U* test; n = 10/treatment).

(H) Representative H&E analysis of lungs from SN25ASP tumor-bearing mice treated with ZA, Doxil, or their combination. Scale bars, 200 μm.

(I and J) Quantitative data on micrometastases were obtained by measuring the size (I) and the number (J) of micrometastases in lungs from treated and untreated mice (LasV program, Leica; *$p < 0.05$; **$p < 0.01$; ***$p < 0.0001$; Mann-Whitney *U* test; n = 10/treatment).

Graphs show mean value plus SEM (upper bar). For additional data, see Figure S7.

R.O. contributed to data interpretation and relevance or provided key reagents.

ACKNOWLEDGMENTS

We thank Dr. Daniele Lecis for critically reviewing the manuscript. The authors thank the Conventional and Confocal Microscopy Facility for confocal images acquisition, the Flow Cytometry Facility for sorting the MDSC subsets, and the Immunohistochemistry Facility for paraffin sections. We also thank Dr. Alessia Burocchi for artwork.

This work was supported by the Associazione Italiana per la Ricerca sul Cancro (My First AIRC Grant 12810 to S.S.; Program Innovative Tools for Cancer Risk Assessment and Diagnosis, 5 per mille number 12162 to C.T. and M.P.C.; and Investigator Grant 10137 to M.P.C.) and the Italian Ministry of Health (grant GR-2013-02355637 to S.S.).

Received: February 3, 2016
Revised: June 3, 2016
Accepted: August 22, 2016
Published: September 27, 2016

REFERENCES

Alique, M., Calleros, L., Luengo, A., Griera, M., Iñiguez, M.A., Punzón, C., Fresno, M., Rodríguez-Puyol, M., and Rodríguez-Puyol, D. (2011). Changes in extracellular matrix composition regulate cyclooxygenase-2 expression in human mesangial cells. Am. J. Physiol. Cell Physiol. *300*, C907–C918.

Bergamaschi, A., Tagliabue, E., Sørlie, T., Naume, B., Triulzi, T., Orlandi, R., Russnes, H.G., Nesland, J.M., Tammi, R., Auvinen, P., et al. (2008). Extracellular matrix signature identifies breast cancer subgroups with different clinical outcome. J. Pathol. *214*, 357–367.

Brekken, R.A., and Sage, E.H. (2001). SPARC, a matricellular protein: at the crossroads of cell-matrix communication. Matrix Biol. *19*, 816–827.

Bronte, V., Brandau, S., Chen, S.H., Colombo, M.P., Frey, A.B., Greten, T.F., Mandruzzato, S., Murray, P.J., Ochoa, A., Ostrand-Rosenberg, S., et al. (2016). Recommendations for myeloid-derived suppressor cell nomenclature and characterization standards. Nat. Commun. *7*, 12150.

Coleman, R.E., Marshall, H., Cameron, D., Dodwell, D., Burkinshaw, R., Keane, M., Gil, M., Houston, S.J., Grieve, R.J., Barrett-Lee, P.J., et al.; AZURE Investigators (2011). Breast-cancer adjuvant therapy with zoledronic acid. N. Engl. J. Med. *365*, 1396–1405.

Collington, S.J., Hallgren, J., Pease, J.E., Jones, T.G., Rollins, B.J., Westwick, J., Austen, K.F., Williams, T.J., Gurish, M.F., and Weller, C.L. (2010). The role of the CCL2/CCR2 axis in mouse mast cell migration in vitro and in vivo. J. Immunol. *184*, 6114–6123.

Danelli, L., Frossi, B., Gri, G., Mion, F., Guarnotta, C., Bongiovanni, L., Tripodo, C., Mariuzzi, L., Marzinotto, S., Rigoni, A., et al. (2015). Mast cells boost myeloid-derived suppressor cell activity and contribute to the development of tumor-favoring microenvironment. Cancer Immunol. Res. *3*, 85–95.

Diel, I.J., Solomayer, E.F., Costa, S.D., Gollan, C., Goerner, R., Wallwiener, D., Kaufmann, M., and Bastert, G. (1998). Reduction in new metastases in breast cancer with adjuvant clodronate treatment. N. Engl. J. Med. *339*, 357–363.

Gabrilovich, D.I., Ostrand-Rosenberg, S., and Bronte, V. (2012). Coordinated regulation of myeloid cells by tumours. Nat. Rev. Immunol. *12*, 253–268.

Gnant, M., Mlineritsch, B., Schippinger, W., Luschin-Ebengreuth, G., Pöstlberger, S., Menzel, C., Jakesz, R., Seifert, M., Hubalek, M., Bjelic-Radisic, V., et al.; ABCSG-12 Trial Investigators (2009). Endocrine therapy plus zoledronic acid in premenopausal breast cancer. N. Engl. J. Med. *360*, 679–691.

Hanahan, D., and Coussens, L.M. (2012). Accessories to the crime: functions of cells recruited to the tumor microenvironment. Cancer Cell *21*, 309–322.

Huang, B., Pan, P.Y., Li, Q., Sato, A.I., Levy, D.E., Bromberg, J., Divino, C.M., and Chen, S.H. (2006). Gr-1+CD115+ immature myeloid suppressor cells mediate the development of tumor-induced T regulatory cells and T-cell anergy in tumor-bearing host. Cancer Res. *66*, 1123–1131.

Huang, X., Dugo, M., Callari, M., Sandri, M., De Cecco, L., Valeri, B., Carcangiu, M.L., Xue, J., Bi, R., Veneroni, S., et al. (2015). Molecular portrait of breast cancer in China reveals comprehensive transcriptomic likeness to Caucasian breast cancer and low prevalence of luminal A subtype. Cancer Med. *4*, 1016–1030.

Kristensen, B., Ejlertsen, B., Mouridsen, H.T., Jensen, M.B., Andersen, J., Bjerregaard, B., Cold, S., Edlund, P., Ewertz, M., Kamby, C., et al. (2008). Bisphosphonate treatment in primary breast cancer: results from a randomised comparison of oral pamidronate versus no pamidronate in patients with primary breast cancer. Acta Oncol. *47*, 740–746.

Lu, P., Weaver, V.M., and Werb, Z. (2012). The extracellular matrix: a dynamic niche in cancer progression. J. Cell Biol. *196*, 395–406.

Lv, D., Zhang, Y., Kim, H.J., Zhang, L., and Ma, X. (2013). CCL5 as a potential immunotherapeutic target in triple-negative breast cancer. Cell. Mol. Immunol. *10*, 303–310.

Lyons, T.R., O'Brien, J., Borges, V.F., Conklin, M.W., Keely, P.J., Eliceiri, K.W., Marusyk, A., Tan, A.C., and Schedin, P. (2011). Postpartum mammary gland involution drives progression of ductal carcinoma in situ through collagen and COX-2. Nat. Med. *17*, 1109–1115.

Mantovani, A., Sozzani, S., Locati, M., Allavena, P., and Sica, A. (2002). Macrophage polarization: tumor-associated macrophages as a paradigm for polarized M2 mononuclear phagocytes. Trends Immunol. *23*, 549–555.

Marigo, I., Bosio, E., Solito, S., Mesa, C., Fernandez, A., Dolcetti, L., Ugel, S., Sonda, N., Bicciato, S., Falisi, E., et al. (2010). Tumor-induced tolerance and immune suppression depend on the C/EBPbeta transcription factor. Immunity *32*, 790–802.

Melani, C., Chiodoni, C., Forni, G., and Colombo, M.P. (2003). Myeloid cell expansion elicited by the progression of spontaneous mammary carcinomas in c-erbB-2 transgenic BALB/c mice suppresses immune reactivity. Blood *102*, 2138–2145.

Melani, C., Sangaletti, S., Barazzetta, F.M., Werb, Z., and Colombo, M.P. (2007). Amino-biphosphonate-mediated MMP-9 inhibition breaks the tumor-bone marrow axis responsible for myeloid-derived suppressor cell expansion and macrophage infiltration in tumor stroma. Cancer Res. *67*, 11438–11446.

Murdoch, C., Muthana, M., Coffelt, S.B., and Lewis, C.E. (2008). The role of myeloid cells in the promotion of tumour angiogenesis. Nat. Rev. Cancer *8*, 618–631.

Obermajer, N., Muthuswamy, R., Odunsi, K., Edwards, R.P., and Kalinski, P. (2011). PGE(2)-induced CXCL12 production and CXCR4 expression controls the accumulation of human MDSCs in ovarian cancer environment. Cancer Res. *71*, 7463–7470.

Perou, C.M. (2010). Molecular stratification of triple-negative breast cancers. Oncologist *15* (*Suppl 5*), 39–48.

Reiman, J.M., Knutson, K.L., and Radisky, D.C. (2010). Immune promotion of epithelial-mesenchymal transition and generation of breast cancer stem cells. Cancer Res. *70*, 3005–3008.

Rodriguez, P.C., Hernandez, C.P., Quiceno, D., Dubinett, S.M., Zabaleta, J., Ochoa, J.B., Gilbert, J., and Ochoa, A.C. (2005). Arginase I in myeloid suppressor cells is induced by COX-2 in lung carcinoma. J. Exp. Med. *202*, 931–939.

Saarto, T., Vehmanen, L., Virkkunen, P., and Blomqvist, C. (2004). Ten-year follow-up of a randomized controlled trial of adjuvant clodronate treatment in node-positive breast cancer patients. Acta Oncol. *43*, 650–656.

Said, N., Socha, M.J., Olearczyk, J.J., Elmarakby, A.A., Imig, J.D., and Motamed, K. (2007). Normalization of the ovarian cancer microenvironment by SPARC. Mol. Cancer Res. *5*, 1015–1030.

Sangaletti, S., Stoppacciaro, A., Guiducci, C., Torrisi, M.R., and Colombo, M.P. (2003). Leukocyte, rather than tumor-produced SPARC, determines stroma and collagen type IV deposition in mammary carcinoma. J. Exp. Med. *198*, 1475–1485.

Sangaletti, S., Tripodo, C., Cappetti, B., Casalini, P., Chiodoni, C., Piconese, S., Santangelo, A., Parenza, M., Arioli, I., Miotti, S., and Colombo, M.P. (2011). SPARC oppositely regulates inflammation and fibrosis in bleomycin-induced lung damage. Am. J. Pathol. *179*, 3000–3010.

Sangaletti, S., Tripodo, C., Sandri, S., Torselli, I., Vitali, C., Ratti, C., Botti, L., Burocchi, A., Porcasi, R., Tomirotti, A., et al. (2014a). Osteopontin shapes immunosuppression in the metastatic niche. Cancer Res. *74*, 4706–4719.

Sangaletti, S., Tripodo, C., Vitali, C., Portararo, P., Guarnotta, C., Casalini, P., Cappetti, B., Miotti, S., Pinciroli, P., Fuligni, F., et al. (2014b). Defective stromal remodeling and neutrophil extracellular traps in lymphoid tissues favor the transition from autoimmunity to lymphoma. Cancer Discov. *4*, 110–129.

Subramanian, A., Tamayo, P., Mootha, V.K., Mukherjee, S., Ebert, B.L., Gillette, M.A., Paulovich, A., Pomeroy, S.L., Golub, T.R., Lander, E.S., and Mesirov, J.P. (2005). Gene set enrichment analysis: a knowledge-based approach for interpreting genome-wide expression profiles. Proc. Natl. Acad. Sci. USA *102*, 15545–15550.

Taube, J.H., Herschkowitz, J.I., Komurov, K., Zhou, A.Y., Gupta, S., Yang, J., Hartwell, K., Onder, T.T., Gupta, P.B., Evans, K.W., et al. (2010). Core epithelial-to-mesenchymal transition interactome gene-expression signature is associated with claudin-low and metaplastic breast cancer subtypes. Proc. Natl. Acad. Sci. USA *107*, 15449–15454.

Toh, B., Wang, X., Keeble, J., Sim, W.J., Khoo, K., Wong, W.C., Kato, M., Prevost-Blondel, A., Thiery, J.P., and Abastado, J.P. (2011). Mesenchymal transition and dissemination of cancer cells is driven by myeloid-derived suppressor cells infiltrating the primary tumor. PLoS Biol. *9*, e1001162.

Tripodo, C., Sangaletti, S., Guarnotta, C., Piccaluga, P.P., Cacciatore, M., Giuliano, M., Franco, G., Chiodoni, C., Sciandra, M., Miotti, S., et al. (2012). Stromal SPARC contributes to the detrimental fibrotic changes associated with myeloproliferation whereas its deficiency favors myeloid cell expansion. Blood *120*, 3541–3554.

Triulzi, T., Casalini, P., Sandri, M., Ratti, M., Carcangiu, M.L., Colombo, M.P., Balsari, A., Ménard, S., Orlandi, R., and Tagliabue, E. (2013). Neoplastic and stromal cells contribute to an extracellular matrix gene expression profile defining a breast cancer subtype likely to progress. PLoS ONE *8*, e56761.

Wilcox, R.A. (2010). Cancer-associated myeloproliferation: old association, new therapeutic target. Mayo Clin. Proc. *85*, 656–663.

Yang, J., Mani, S.A., Donaher, J.L., Ramaswamy, S., Itzykson, R.A., Come, C., Savagner, P., Gitelman, I., Richardson, A., and Weinberg, R.A. (2004). Twist, a master regulator of morphogenesis, plays an essential role in tumor metastasis. Cell *117*, 927–939.